# SANDIA REPORT

SAND2000-0396
Unlimited Release
Printed February 2000



# Characterization of the Li(Si)/$CoS_2$ Couple for a High-Voltage, High-Power Thermal Battery

Ronald A. Guidotti and Frederick W. Reinhardt

Prepared by
Sandia National Laboratories
Albuquerque, New Mexico 87185 and Livermore, California 94550

Sandia is a multiprogram laboratory operated by Sandia Corporation, a Lockheed Martin Company, for the United States Department of Energy under Contract DE-AC04-94AL85000.



Sandia National Laboratories

Issued by Sandia National Laboratories, operated for the United States Department of Energy by Sandia Corporation.



Available to DOE and DOE contractors from
U.S. Department of Energy
Office of Scientific and Technical Information
P.O. Box 62
Oak Ridge, TN 37831

Telephone: (865)576-8401
Facsimile: (865)576-5728
E-Mail: reports@adonis.osti.gov
Online ordering: http://www.doe.gov/bridge

Available to the public from
U.S. Department of Commerce
National Technical Information Service
5285 Port Royal Rd
Springfield, VA 22161

Telephone: (800)553-6847
Facsimile: (703)605-6900
E-Mail: orders@ntis.fedworld.gov
Online order: http://www.ntis.gov/ordering.htm

## DISCLAIMER

Portions of this document may be illegible in electronic image products. Images are produced from the best available original document.

SAND2000-0396
Unlimited Release
Printed February 2000

# Characterization of the Li(Si)/$CoS_2$ Couple for a High-Voltage, High-Power Thermal Battery

Ronald A. Guidotti and Frederick W. Reinhardt
Power Sources Engineering and Development Department
Sandia National Laboratories
P.O. Box 5800
Albuquerque, NM 87185-0614

## Abstract

In order to determined the capabilities of a thermal battery with high-voltage and high-power requirements, a detailed characterization of the candidate LiSi/LiCl-LiBr-LiF/$CoS_2$ electrochemical couple was conducted. The rate capability of this system was investigated using 0.75"- and 1.25"-dia. single and multiple cells under isothermal conditions, where the cells were regularly pulsed at increasingly higher currents. Limitations of the electronic loads and power supplies necessitated using batteries to obtain the desired maximum current densities possible for this system. Both 1.25"- and 3"-dia. stacks were used with the number of cells ranging from 5 to 20. Initial tests involved 1.25"-dia. cells, where current densities in excess of 15 A/$cm^2$ (>200 W/$cm^2$) were attained with 20-cell batteries during 1-s pulses. In subsequent follow-up tests with 3"-dia., 10-cell batteries, ten 400-A, 1-s pulses were delivered over an operating period of ten minutes. These tests formed the foundation for subsequent full-sized battery tests with 125 cells with this chemistry.

## Acknowledgments

The authors wish to acknowledge the assistance of Greg Scharrer, 2553, who was the design engineer for the final battery.

# Contents



# Figures

## Tables

# Characterization of the Li(Si)/$CoS_2$ Couple for a High-Voltage, High-Power Thermal Battery

## Introduction

Thermal batteries are ideally suited for applications where there is a need for high reliability and high power. The basis for the high-power capability lies with the high ionic conductivity of the molten salt used in the separator. Using a bipolar stack design, various voltages and currents are possible by including the requisite number of cells in a battery stack and by placing battery stacks in series or parallel, depending on the design requirements.

Sandia was approached by an outside customer to design and develop a thermal battery that was beyond the limits normally used for this technology. A high-voltage, high-power battery was required for a DC-to-DC power-conditioning unit. The battery was to deliver multiple 360-A pulses of between one and five seconds duration at a working voltage of 500 V—a power delivery of 180 kW—over an operating time of 10-15 minutes. A specific power of at least 7 kW/kg was targeted.

For this application, the all-Li LiCl-LiBr-LiF electrolyte was selected because of its intrinsic high $Li^+$ conductivity. The anode selected was based on 44% Li/56% Si alloy and the cathode was based on $CoS_2$ because of its high-rate capability. This is similar to the chemistry for potential future sonobuoy applications that Northrop-Grumman has been developing, except that a low-melting electrolyte was used for that application, in order to provide a long operating life.[1] The power required for the sonobuoy applications was 4.2 kW. In the present work, it was necessary to achieve almost 36 times greater power.

To meet the requirements of the envisioned inverter application, the original battery design involved connecting four modules in series. Each module would use a 3"-dia. battery stack containing 125 cells and would have an overall diameter of 4" and a length of 11". This design resulted in a 45 kW battery module at a load current of 360 A and a nominal voltage of 1 V/cell.[2]

The initial study focused on determining the limitations of the electrochemical couple. This involved testing multiple cells isothermally, as well as in 5-, 10-, and 20-cell batteries. Initial tests involved 1.25"-dia. cells and subsequent follow-up tests used 3"-dia., 5-cell batteries. Ultimately, 125-cell modules were tested. This report will describe the results of these screening and characterization tests.

# Experimental Procedures

## Test Procedures

The cells were assembled in the dry room and were tested using temperature-controlled heated platens in a glovebox where the moisture and oxygen levels were each maintained at <10 ppm. The cells were tested under computer control at temperatures of 450°C to 550°C under constant-current conditions using a HP6060B electronic load rated at 60 A or 300 W. A limited number of tests were also conducted using a Kepco 20-A/20-V bipolar power supply. The cells were tested under open-circuit conditions with a 1-s pulse applied every 10 s. The pulse current was incremented with each pulse until either the load saturated or the maximum current density was reached. Due to poor regulation of the electronic load when testing single cells under these high-current conditions, it was necessary to test two and three cells in series, to increase the voltage.

Tests were also performed under constant resistance using a HP8116 function generator to trigger a MOSFET to place the load across the cell for 1 s every 10 s. This technique was limited to the minimum resistance that could be placed across the cell. Even with a dead short, the resistance of the MOSFET junction of 0.27 ohms was still too high. Because of this, this test procedure was abandoned.

Battery tests were conducted using a reusable test fixture that could handle five to more than 20 cells. Preliminary tests were done using 1.25"-dia. cells (7.92 $cm^2$ area). Later tests used the 3"-dia. stacks (45.6 $cm^2$) in the reusable fixture shown in Figure 1. Prototype batteries were then assembled using a "built-up" header and a conventional welded case. All the battery tests incorporated a thermocouple to measure the stack temperature during discharge (at the cell closest to the base end, opposite the header). Electrical connections to the header feedthroughs were made with 1/2"-wide Cu braid. The current collectors used were 0.010"-thick Cu discs that were brazed to the Cu braid. The batteries were tested using 1.5-kW and 4.0-kW electronic loads (Transistor Devices, Inc.). The 1.5-kW load was rated at 100 A at up to 200 V, while the 4-kW unit was rated at 400 A at up to 600 V. For testing of the full 125-cell battery module, a Vespel® insert was epoxied into a machined conventional header. The insert held tapered ¼"-dia. copper rods which served as the electrical feedthroughs. Electrical connection from the stack to the feedthroughs was made via copper current collectors and braid. The braid was attached to the feedthroughs and current collectors by high-temperature silver solder. Figure 2 shows a picture of the parts before assembly into the battery.

## Materials

The flooded anodes used contained 25% electrolyte and 44% Li/56% Si and had a mass of 0.93 g. The separator was based on the LiCl-LiBr-LiF minimum-melting composition with 35% MgO (Merck Maglite S) and varied in thickness from 0.010" to 0.21". The catholyte contained 73.5% $CoS_2$/25% separator/1.5% $Li_2O$ and has a mass of 1.15 g. It was pressed onto a graphite paper substrate to act as a current collector as well as a reinforcing member. Single cells 1.25" in diameter were assembled from cold-pressed

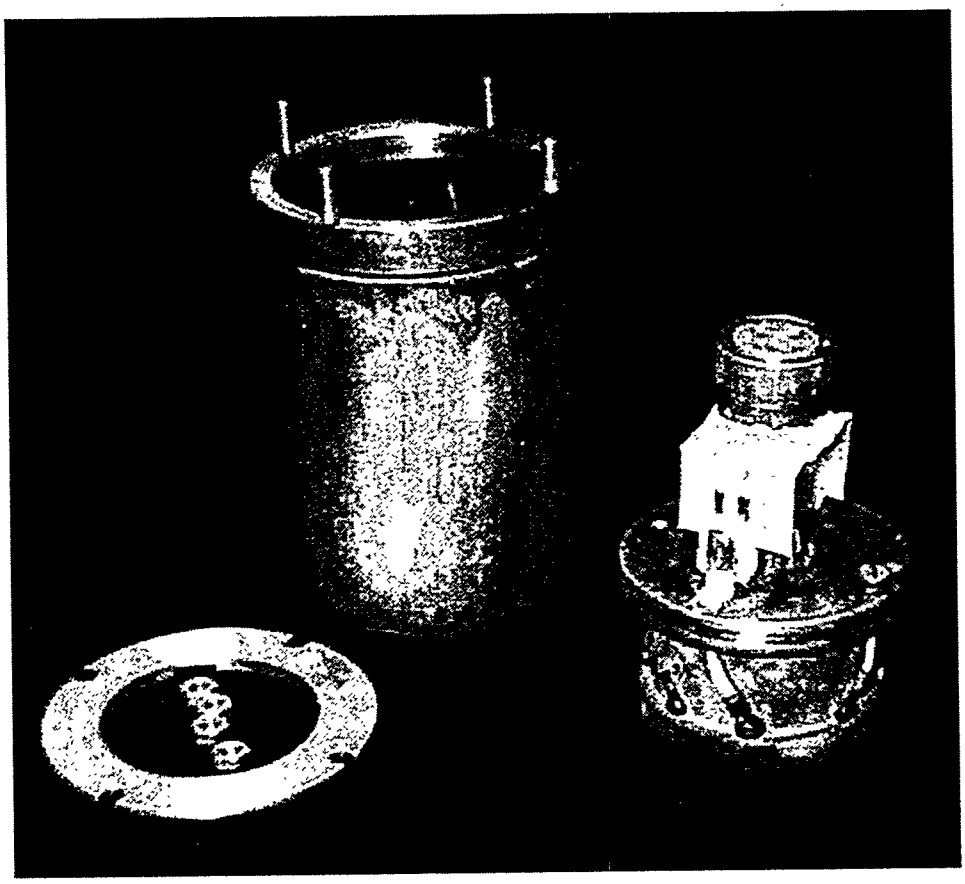

Figure 1. Reusable Test Fixture Used with 3"-Diameter Battery Stacks.

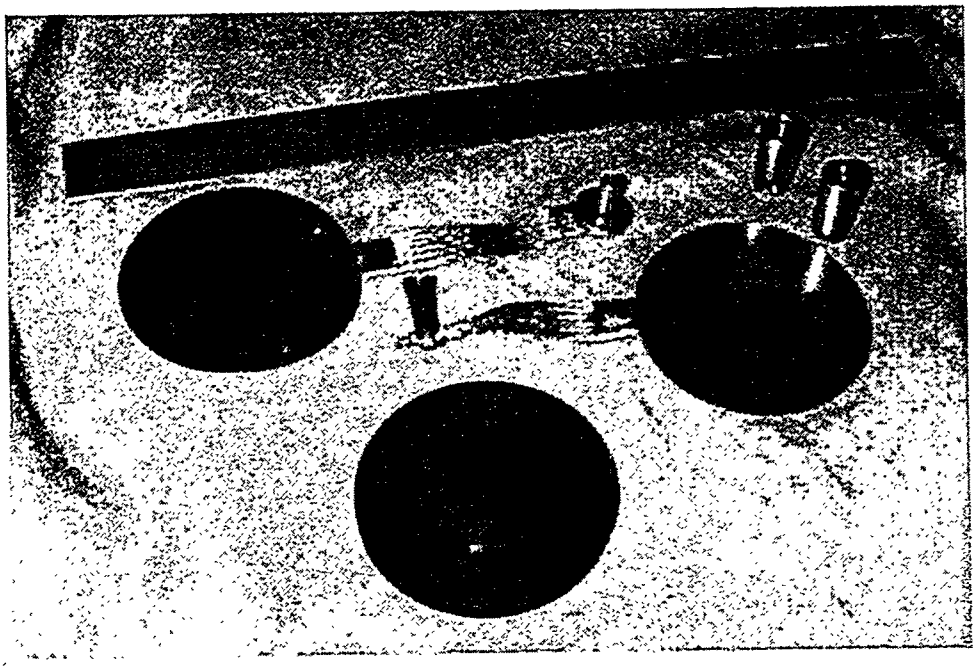

Figure 2. Piece Parts Used in Header Incorporating Vespel® Insert.

anode, separator, and cathode pellets. Similarly, cell stacks containing two and three cells were also tested, when single cells proved inadequate.

## Results and Discussion

### Isothermal Cell Tests

The intent of these tests was to try to determine the highest current density that a cell could sustain for a given temperature. The load was applied as a 1-s pulse every 10 s while the cell was on open circuit and was incremented by a fixed amount at each successive pulse. A typical response at 450°C for a double 1.25"-dia., LiSi/LiCl-LiBr-LiF/$CoS_2$ cell is shown in Figure 3 for the case where 0.021"-thick separators were used and where the pulse current was incremented in 1-A steps. The current plateaued at about 2.3 A/cm$^2$ (18.4 A) at about 180 s; the maximum power density for this test was about 5 W/cm$^2$. The minimum voltage during the pulses showed a corresponding decrease with a similar plateau near 2.16 V. The limiting current density in this case is not representative of the cell but is a reflection of the inability of the load to sink any higher current. This is indicated by the corresponding plateau in the minimum cell voltage vs. time. Thus, these data represent limitations imposed by the electronic load used for this test.

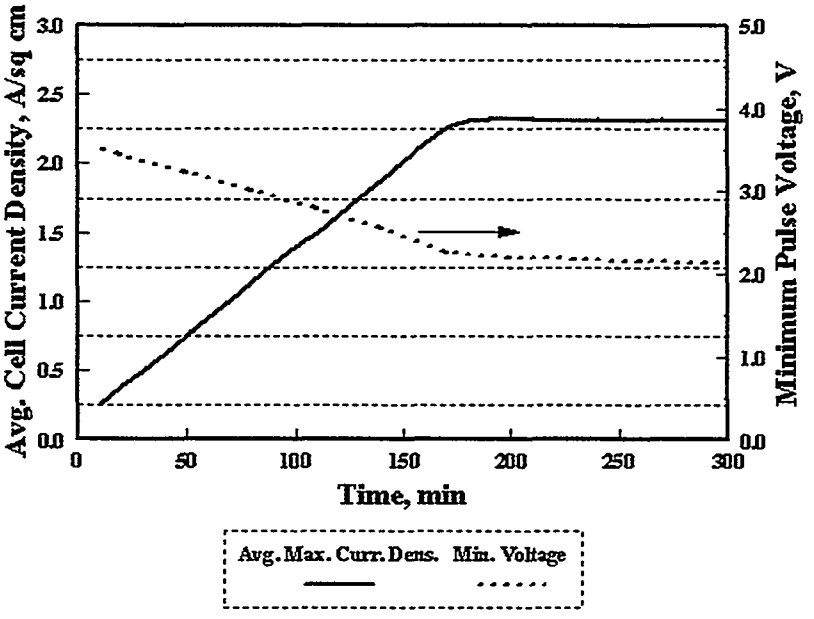


Figure 3. Average Current Density and Minimum Pulse Voltage during Discharge of Double LiSi/LiCl-LiBr-LiF/$CoS_2$ Cell During 1-s Pulses at 450°C.

The tests were repeated at 500°C but with a double cell that was smaller in diameter (0.75"), to increase the current density for the same limiting current. For this test, a limiting current density of 5 A/cm$^2$ was attained, with a corresponding power density of 8.6 W/cm$^2$. Unfortunately, the same plateauing behavior in the maximum cell current

density and minimum voltage still occurred. This indicated that the electronic load was still saturating under these conditions. Attempts to use the 20-A Kepco bipolar power supply were similarly unsuccessful. Whenever the current would reach ~16 A, the power supply would go into an overload condition, thus making it unsuitable for this application.

Next, the use of a triple-cell stack was examined with both 0.75"- and 1.25"-diameter pellets over a temperature range of 450° to 550°C. This was near the limit for cell heating using the present test fixture, due to space constraints and heat losses with larger platen spacings. The results of these tests are summarized in Table 1, along with the data for the double-cell tests.

Table 1. Summary of Test with Double and Triple Cells.

| Temperature, °C | No. Cells | Cell Dia., in | Limiting Current Density, mA/cm² | Limiting Min. Voltage per Cell, V | Limiting Power Density, W/cm² | Coulombs Extracted |
|---|---|---|---|---|---|---|
| 450 | 2 | 1.25 | 2.32 | 1.103 | 5.17 | 408 |
| 500 | 2 | 0.75 | 5.01 | 0.846 | 8.60 | 276 |
| 450 | 3 | 1.25 | 3.46 | 0.729 | 8.00 | 373 |
| 500 | 3 | 1.25 | 3.66 | 0.782 | 9.03 | 470 |
| 550 | 3 | 1.25 | 3.51 | 0.963 | 10.3 | 376 |
| 450 | 3 | 0.75 | 4.01 | 0.463 | 6.64 | 106 |
| 500 | 3 | 0.75 | 6.94 | 0.742 | 16.4 | 398 |
| 550 | 3 | 0.75 | 7.70 | 0.797 | 18.9 | 243 |

The limiting-current densities and limiting-power densities are plotted as a function of temperature and number of cells in the stack in Figure 4 and 5, respectively, for the two sizes of pellets. The limiting current was increased to 7.7 A/cm² for the 0.75"-dia. cell at the highest temperature of 550°C, with a corresponding power density of 18.9 W/cm². If the electronic loads were the sole cause of the limiting current, one would expect no temperature dependence. This was the case for the limiting current densities for the 1.25"-dia. triple cells but not for the 0.75"-dia. cells. The power densities showed greater temperature dependence.

The capacities of the various cells under the above test conditions are summarized in Figure 6. As expected, the capacities showed pronounced temperature dependence, as the rate capabilities are enhanced at elevated temperatures. The drop in capacity at 550°C may be due to increased solubility of the Li(Si) or $CoS_2$ in this electrolyte at this

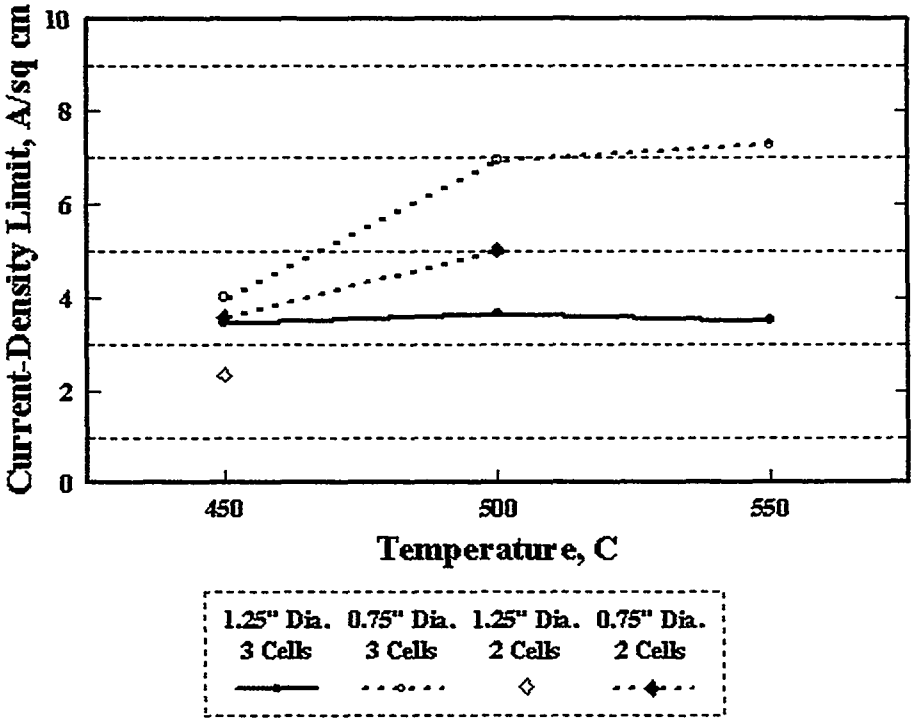


Figure 4. Limiting Current Densities for Multiple-Cell LiSi/LiCl-LiBr-LiF/$CoS_2$ Stacks as a Function of Temperature and Cell Diameter

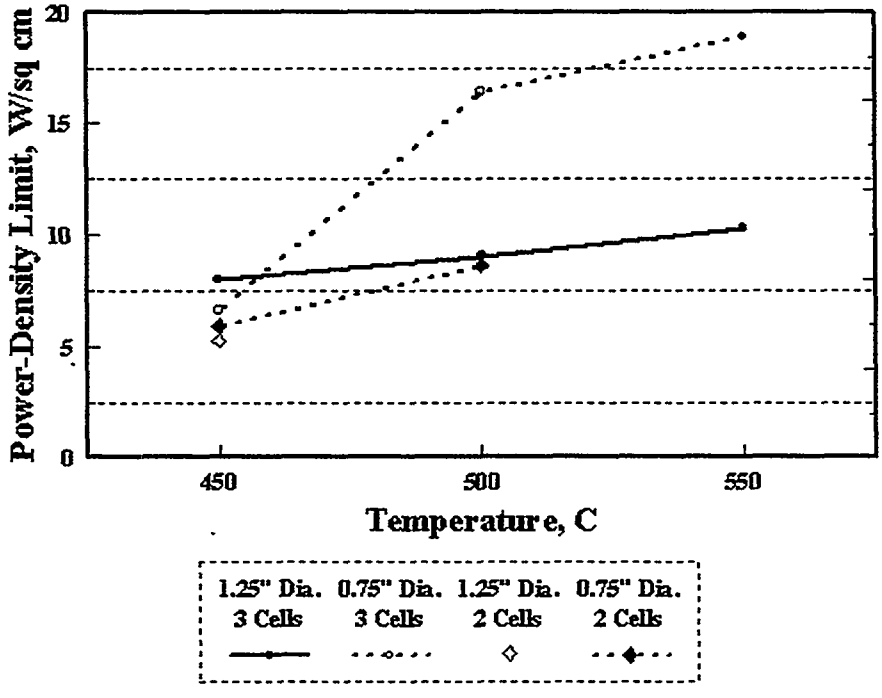


Figure 5. Limiting Power Densities for Multiple-Cell LiSi/LiCl-LiBr-LiF/$CoS_2$ Stacks as a Function of Temperature and Cell Diameter.

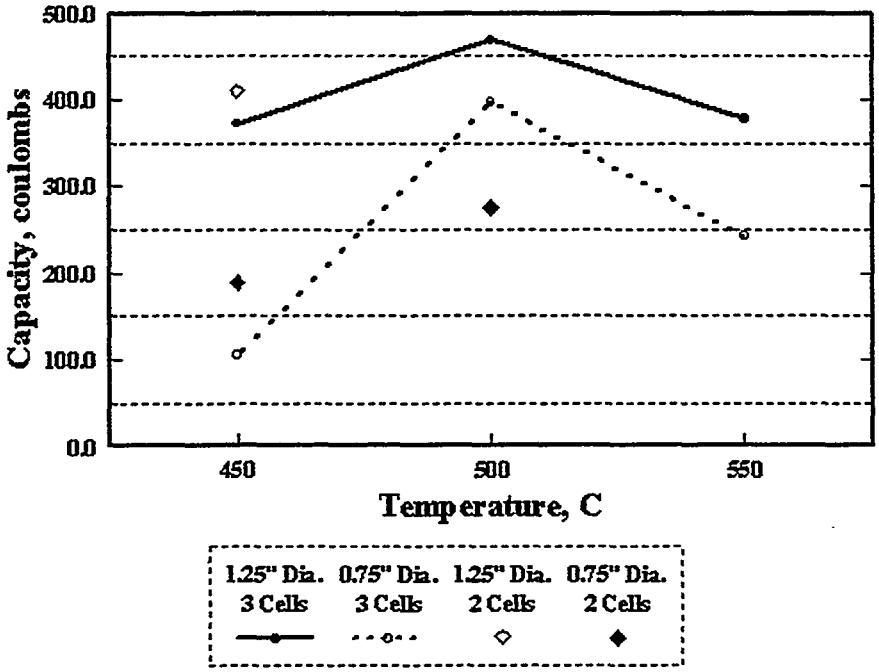


Figure 6. Capacities of LiSi/LiCl-LiBr-LiF/$CoS_2$ Double and Triple Cells as a Function of Temperature and Cell Diameter.

temperature. Similar behavior has been observed with $FeS_2$ in the all-Li system.[3] The corresponding minimum cell voltages for these tests are summarized in Figure 7.

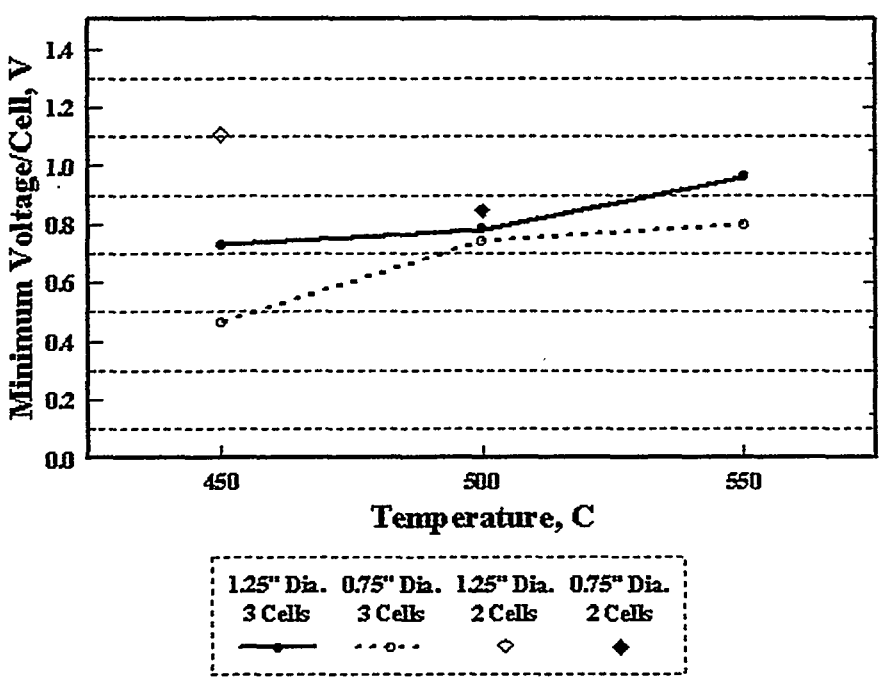


Figure 7. Minimum Cell Voltages of LiSi/LiCl-LiBr-LiF/$CoS_2$ Double and Triple Cells as a Function of Temperature and Cell Diameter.

These data suggest that even smaller cells would be necessary to reach the true limiting current densities for this system. Since the use of smaller cells or a larger number of cells with the "single-cell" tester were not practical, it was decided to go directly to batteries for determination of the rate capability of the LiSi/LiCl-LiBr-LiF/$CoS_2$ system

## Battery Tests

**5-Cell, 1.25"-Dia. Batteries**. The initial battery tests were conducted using 1.25"-diameter stacks that were insulated with four wraps of 0.080"-thick Fiberfrax® ceramic blanket. Two 5-cell batteries were built and tested with the 1.5 kW electronic load. The programmed current was set to 50 A, which is well above what the batteries could actually deliver, to drive the system to its maximum rate capability. Both batteries were activated at 74°C; one used a heat balance of 102.5 cal/g and the second used 104.8 cal/g. These tests were done with a standard reusable test fixture that employed stainless steel current collectors and iron leads that connect to the current feedthroughs in the header.

Since the battery temperature drops with time because of thermal losses, the corresponding maximum current and power density will similarly decrease. The highest average current density was only 4.1 A/cm$^2$ (at the start of discharge) for the battery with the lower heat balance and 5.0 A/cm$^2$ for the one with the higher heat balance. This is lower than the highest values noted for the double- and triple-cell tests (Table 1). The corresponding minimum voltages during the pulses on a per-cell basis, however, were higher, resulting in an increased power density.

To minimize IR losses, a larger test fixture for the subsequent battery tests was used that incorporated heavy copper leads and current collectors at the ends of the stack. In addition, a 3/8"-thick Min-K® TE1400 sleeve was used in place of the ceramic blanket wrap. With the improved insulation, a lower heat balance of 100.5 to 102.5 cal/g was used and the batteries were activated at ambient temperature. The larger test fixture was used to test both 5-cell and 20-cell batteries with the larger 4-kW electronic load.

There was some concern about using copper in direct contact with the LiSi anode. The possibility of alloy formation was examined by differential scanning calorimetry (DSC) in a Mo pan under high-purity argon. The results of the DSC tests, shown in Figure 8, indicate that the Cu reacts exothermically with LiSi (after an initial endotherm) at temperatures above 620°C. To avoid this reaction in the batteries, a 0.005"-thick 304 stainless steel disc was used between the anode and the Cu current collector.

The results of the tests with the 1.25"-diameter batteries are summarized in Table 2. Where possible, data for temperatures of 450°, 500°, and 550°C were extracted using the temperature-time curves as a basis. Data for the first pulse are also indicated where appropriate. When the system was below its rate-limiting current density, the maximum current density occurred during this first pulse. The pulse current was incremented only for the last 20-cell test (Test No. 5).

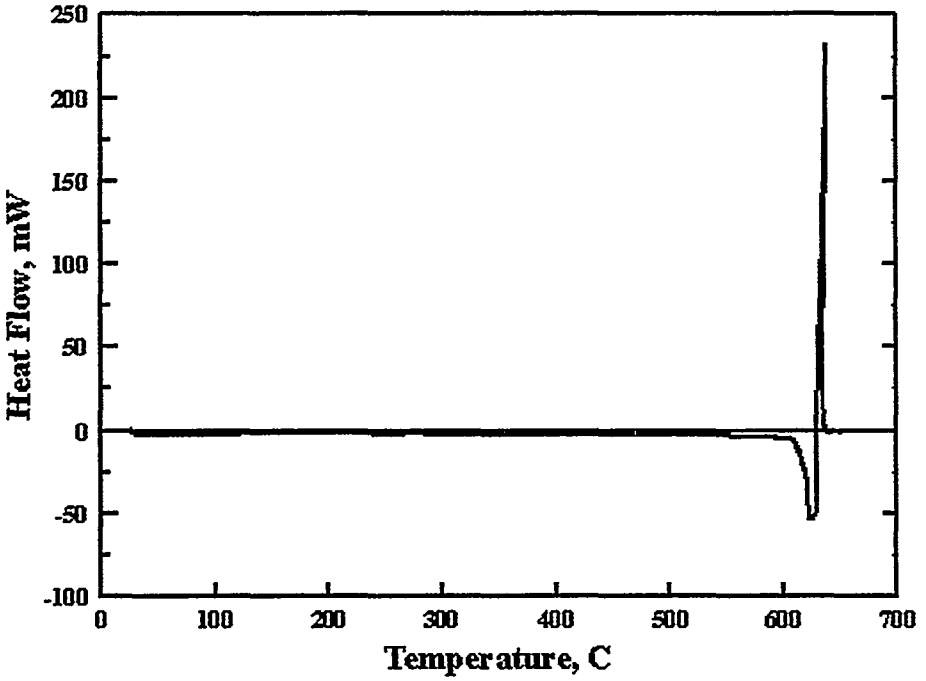


Figure 8. DSC Trace of Reaction of Powdered LiSi Anode with Cu Powder.

With the 5-cell batteries, the rate-limiting current density depended strongly on temperature, as shown in Figure 9, for the old test fixture. The corresponding power densities are plotted in Figure 10. The maximum current and power densities delivered were almost directly proportional to the stack temperature. This is not surprising, as the kinetics would be enhanced at the higher temperatures and the electrolyte conductivity would similarly be greater under the same conditions.

For these tests, the pulsing current was not incremented but was set in the computer program to be well above the expected value that the battery could deliver. Thus, the load was trying to sink more current than the battery could supply. Under these circumstances, the highest current density was delivered during the first pulse. The highest power that was delivered during the tests with the old test fixture was about 15 W/cm$^2$.

**20-Cell, 1.25"-Dia. Batteries.** Better results were obtained when using the improved test fixture with Cu connectors and current collectors with a 20-cell stack. Compared to the 5-cell stacks, the minimum voltage per cell was much higher for the first 20-cell battery (Test 4 of Table 2) and the current density that could be sustained was much higher. This battery used a heat balance of 104.8 cal/g and was activated at 74°C. The value of 3.81 A/cm$^2$, however, was not the true limiting current density but was set by the computer program at the start of the test. At the time, it was felt that the battery would probably not be able to actually deliver this high a current density. Otherwise, a higher current level would have been set. The corresponding power density was 208 W/cm$^2$, which was the highest recorded at the time.

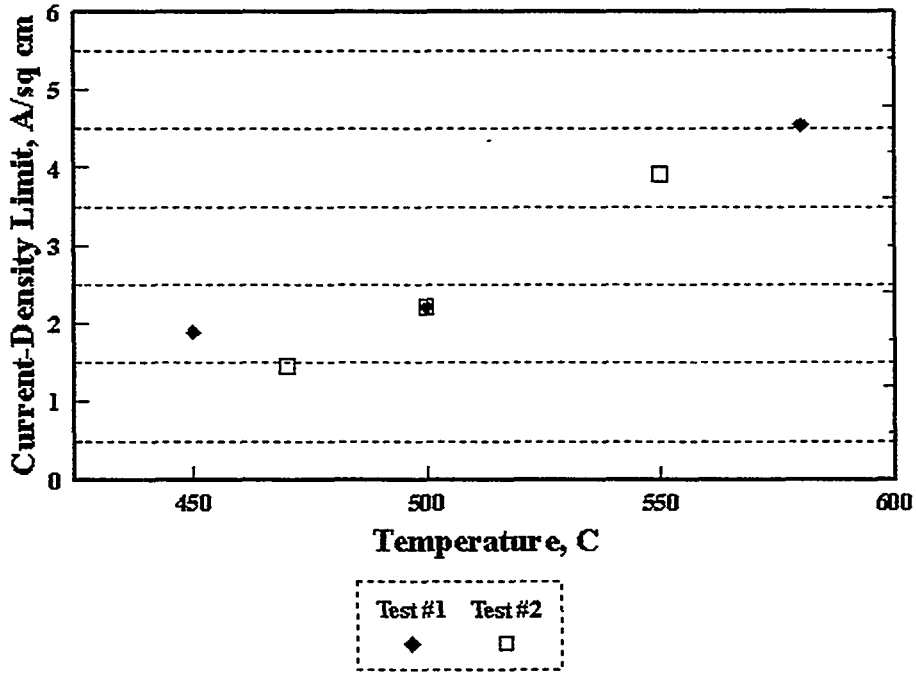


Figure 9. Limiting Current Densities for 1.25"-Dia., 5-Cell LiSi/LiCl-LiBr-LiF/$CoS_2$ Batteries as a Function of Temperature During Discharge.

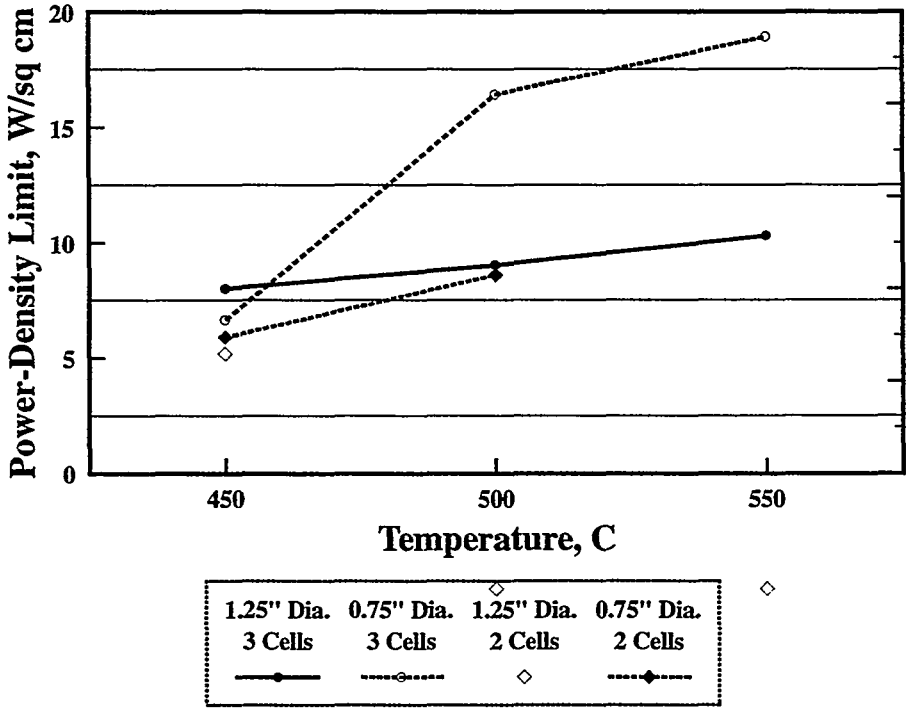


Figure 10. Limiting Power Densities for 1.25"-Dia., 5-Cell LiSi/LiCl-LiBr-LiF/$CoS_2$ Batteries as a Function of Temperature During Discharge.

In the next 20-cell test (Test 5 in Table 2), the current was ramped with each pulse until the highest value was recorded. The current density and minimum pulse voltage vs. time are shown in Figure 11 and the corresponding battery polarization (resistance) and thermal profile are shown in Figure 12. (The early temperature data were lost due to a malfunction of the thermocouple reference junction.) At the highest current density, the battery current was over 131 A, which the test fixture could easily handle for these short pulses. At ~125 s, the current and voltage dropped as the load could no longer regulate at this high-power level. At ~270 s, the battery began to overheat from the large IR heating, and went into a thermal runaway.

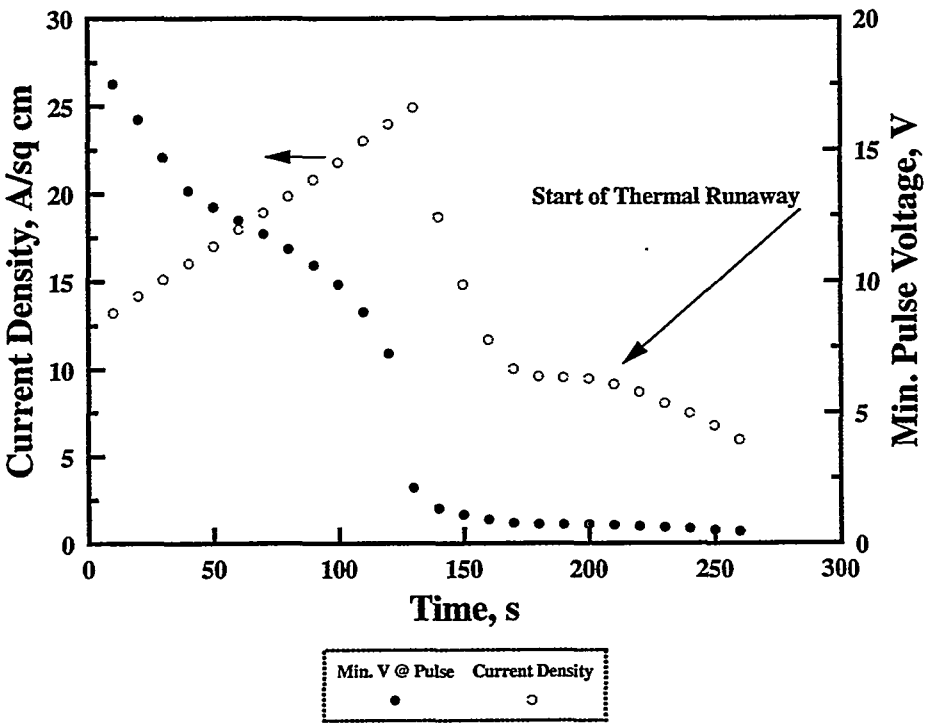


Figure 11. Current Density and Minimum Pulse Voltage for 1.25"-Dia., 20-Cell LiSi/LiCl-LiBr-LiF/$CoS_2$ Battery during High-Current Pulse Discharge.

The battery polarization increased rapidly after ~130 s, which severely limited the power output. *It should be noted that the battery resistance includes connector and lead resistances as well as interfacial resistances and polarization contributions and, as such, is a composite of the entire system.* The resistive contribution of the test fixture was reduced using heavy gauge Cu connectors. The use of Cu current collectors and leads in the battery stack minimized IR losses, as well.

The highest current density attained in Test 5 was 16 A/cm$^2$. However, at this level, the polarization was so great—as evidenced by the low minimum voltage per cell—that the actual power delivered was less than that for Test 4. A better indicator of the battery performance is a plot of the power density vs. the minimum battery voltage during the pulses. These data are presented in Figure 13. The power density shows a maximum of 220 W/cm$^2$ near a minimum battery voltage of ~17 V (~0.85 V/cell) after the initial first

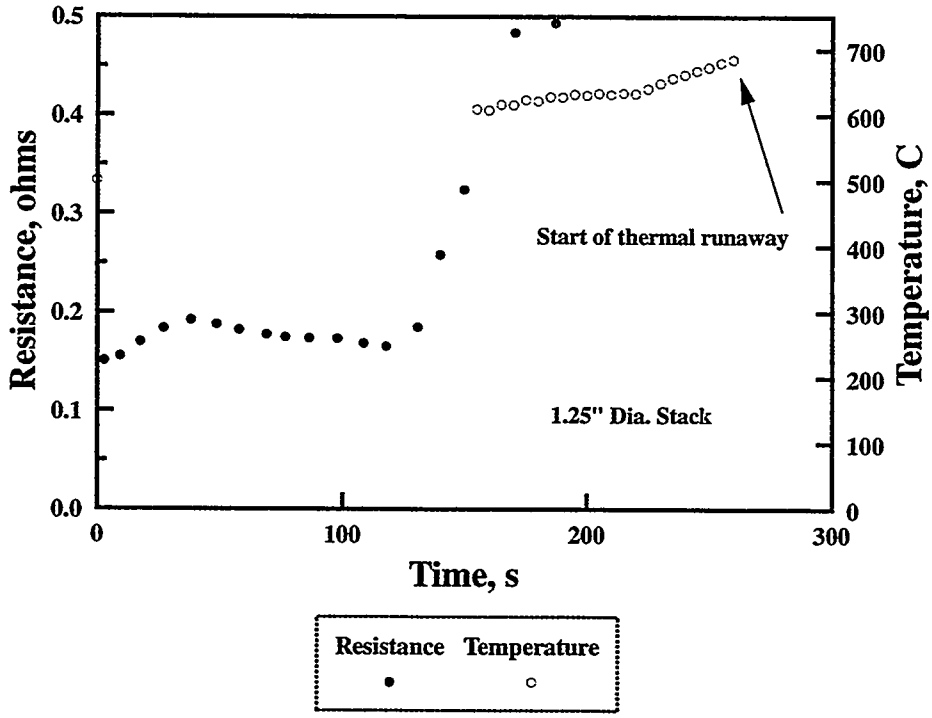


Figure 12. Resistance and Internal Temperature for 1.25"-Dia., 20-Cell LiSi/LiCl-LiBr-LiF/$CoS_2$ Battery during High-Current Pulse Discharge.

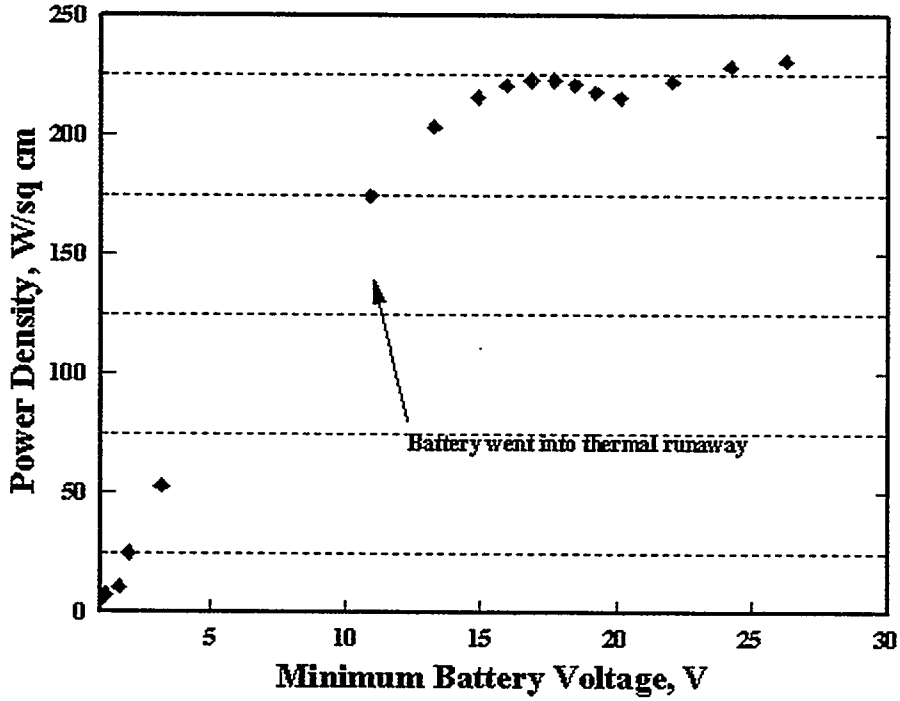


Figure 13. Power Density for 1.25"-Dia., 20-Cell LiSi/LiCl-LiBr-LiF/$CoS_2$ Batteries as a Function of Minimum Pulse Voltage.

pulse which had the largest power output of 1.83 kW. The voltage fell drastically when the battery went into thermal runaway at the point indicated.

In the next 20-cell test, the heat balance was further reduced to 100.2 cal/g and the battery was activated at room temperature (Test 6 in Table 2). This battery was tested at a constant pulse level of 80 A (10.1 A/ $cm^2$). This fixed the amount of IR heating during the test which prevented the battery from going into thermal runaway, as did the first two 20-cell batteries. While the battery temperature gradually increased during discharge, it never exceeded 600°C. Still, a power density of 250 W/ $cm^2$ was attained in the test, which was higher than that for the first 20-cell test.

Progressively increasing the pulse current results in a steady increase in the IR heating during the pulse, although the pulse is only 1 s long. With the Min-K® insulation, the heat losses are considerably reduced compared to the ceramic-blanket (Fiberfrax®) wrap. Consequently, thermal management is critically important when designing batteries for high-power applications. This becomes even more important as the length and diameter of the battery are increased.

The relative thermal characteristics of the 5-cell and 20-cell batteries are compared in Figure 14. The stack temperature for Test 2, for the 5-cell battery, showed the typical peak early in life followed by a gradual cooling. This battery used the ceramic blanket wrap and had a slightly higher heat balance, resulting in the higher maximum stack temperature. In Test 3, however, the stack temperature was not as great and did not peak until 320 s into discharge. This reflects the use of the Min-K® sleeve, which is a much better insulation, and the slightly higher power density attained during this run.

The temperature for the first 20-cell battery (Test 4), activated at 74°C, exhibited a high value early in discharge and stayed well above 650°C—the temperature where thermal decomposition of $CoS_2$ becomes significant—for 150 s. At that time, the battery rapidly went into a thermal-runaway condition. This battery used a heat balance of 104.8 cal/g and a Min-K® sleeve. The heat balance was reduced to 102.5 cal/g for the next 20-cell battery (Test 5) that was activated at room temperature. In this test, the current during discharge was progressively increased with each pulse, which caused rapid build-up of IR heating, leading to thermal runaway at 270 s. The third 20-cell battery (Test 6) was also activated at room temperature but with a further reduction in the heat balance to 100.2 cal/g. The temperature profile for this battery showed a gradual heating throughout discharge, reaching 600°C at 890 s. It did not go into thermal runaway.

The temperatures for the 20-cell batteries were much higher than the temperatures generated with the 5-cell batteries because of the much higher IR heating during discharge. The high IR heating, coupled with the Min-K® insulation, caused a rapid buildup of heat in the battery stack, until thermal decomposition of $CoS_2$ became excessive, resulting in the generation of elemental sulfur. The fugitive sulfur vapor then rapidly reacted exothermically with the porous LiSi anode.

**Table 2.** Summary of Test with 1.25"-Diameter Batteries.

| Test No. | Test Fixture | Insul. | Heat Balance, cal/g | Activ. Temp., °C | Max. Stack Temp., °C | Stack Temp., °C* | Time Between Pulses, s | No. of Cells | Limiting Current Density, A/cm² | Limiting Minimum Voltage/ Cell, V | Power Dens. @ Limit. Curr. Dens., W/cm² |
|---|---|---|---|---|---|---|---|---|---|---|---|
| 1 | Old (SS) | Fiberfrax® | 102.5 | 74 | 530 | 450 | 10 | 5 | 1.89 | 0.30 | 2.84 |
| | | | | | | 500 | | | 2.21 | 0.58 | 6.40 |
| | | *1st Pulse:* | ---> | | | *580* | | | *4.55* | *0.806* | *18.3* |
| 2 | Old (SS) | Fiberfrax® | 104.8 | 74 | 587 (@ 40 s) | 470 | 10 | 5 | 1.45 | 0.293 | 2.12 |
| | | | | | | 500 | | | 2.21 | 0.368 | 4.07 |
| | | | | | | 550 | | | 3.91 | 0.657 | 12.8 |
| | | *1st Pulse:* | ---> | | | *525* | | | *4.28* | *0.700* | *15.0* |
| 3 | Old (SS) | Min-K® | 102.5 | 22 | 560 (@ 305 s) | 516 *(1st pulse)* | 10 | 5 | 5.15 | 0.536 | 13.8 |
| 4 | New (Cu) | Min-K® | 104.8 | 74 | >700 (@ 270 s) | 710 | 10 | 20 | 3.81# | 1.38 | 208.4 |
| 5 | New (Cu) | Min-K® | 102.5 | 22 | >700 (@ 130 s) | 590 | 10 | 20 | 16.0 | 0.160 | 174.3 |
| 6 | New (Cu) | Min-K® | 100.2 | 22 | 600 (@ 895 s) | 486 | 30 | 20 | 10.1# | 1.24 | 250 |

* Temperatures taken from temperature-time trace during discharge.
# Limited by program and not battery.

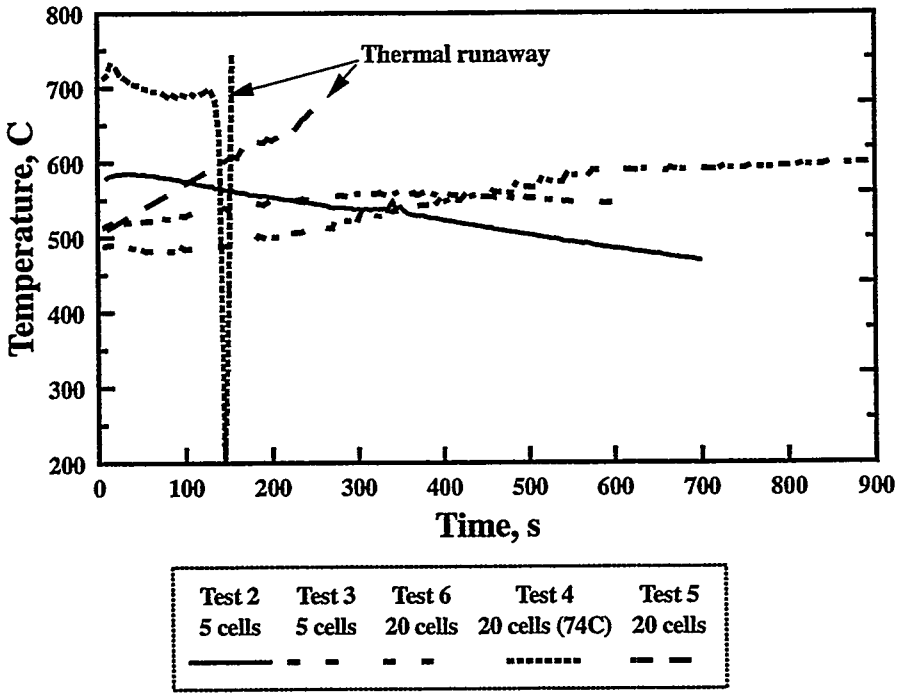


Figure 14. Comparison of Thermal Profile of Battery Stacks for 1.25"-Dia. 5-Cell and 20-Cell LiSi/LiCl-LiBr-LiF/$CoS_2$ Batteries.

During discharge, the cathode undergoes the following electrochemical reaction:

$$CoS_2 + 4/3\ e^- \text{ -----> } 1/3\ Co_3S_4 + 2/3\ S^{-2} \quad [1]$$

The open-circuit voltage of the LiSi/$CoS_2$ couple for this reaction is 1.85 V at 500°C. However, at temperatures above 650°C, the $CoS_2$ thermally decomposes to form lower sulfides of Co and elemental sulfur vapor according to equations 2 and 3.

$$3CoS_{2(s)} \text{ -----> } Co_3S_{4(s)} + S_{2(v)} \quad [2]$$

The $Co_3S_4$ can further decompose to a second lower sulfide of Co:

$$3Co_3S_{4(s)} \text{ -----> } Co_9S_{8(s)} + 2S_{2(v)} \quad [3]$$

The overall final reaction is then given by equation 4:

$$9CoS_{2(s)} \text{ -----> } Co_9S_8 + 5S_{2(v)} \quad [4]$$

The sulfur vapor rapidly reacts with the LiSi to generate a large amount of heat, as shown in equation 5 for the actual anode composition:

$$2Li_{13}S_{4(s)} + 14.5S_{2(v)} \text{ -----> } 13Li_2S_{(s)} + 8SiS_{2(s)} \quad [5]$$

The amount of heat released in this reaction is of the order of over hundreds of kilocalories per mole of $Li_{13}Si_4$. If a complete thermal runaway occurs, the reaction can become so intense as to

melt the stainless steel case and burn a hole through the side of the can, allowing access to atmospheric oxygen and moisture which will further fuel additional exothermic oxidation reactions. The very real possibility of thermal runaway adds greatly to the safety concerns in testing large thermal batteries of this type.

The battery resistance on a per-cell basis is compared for the various 5-cell and 20-cell stacks in Figure 15. All the curves show similar behavior, with a small hump in resistance near 300 s—the time will vary depending on the capacity extracted—which reflects the slight increase in resistance of the discharge phase, $Co_3S_4$. After that, there is a gradual increase in resistance with discharge time, most likely reflecting the increased polarization and mass transfer within the fine particles of discharged $CoS_2$. Traditional concentration gradients as would be common in the LiCl-KCl eutectic are absent here, due to the lack of any aliovalent cations. In the latter case, the rapid build up of Li ions at the separator-anode interface results in a rapid increase in the melting point of the electrolyte, as the composition moves off the eutectic. This caused solids to precipitate which results in less liquid for mass transfer and a higher resistance path through the cell. In the case of the all-Li electrolyte, there is still the possibility of polarization caused by migration effects.

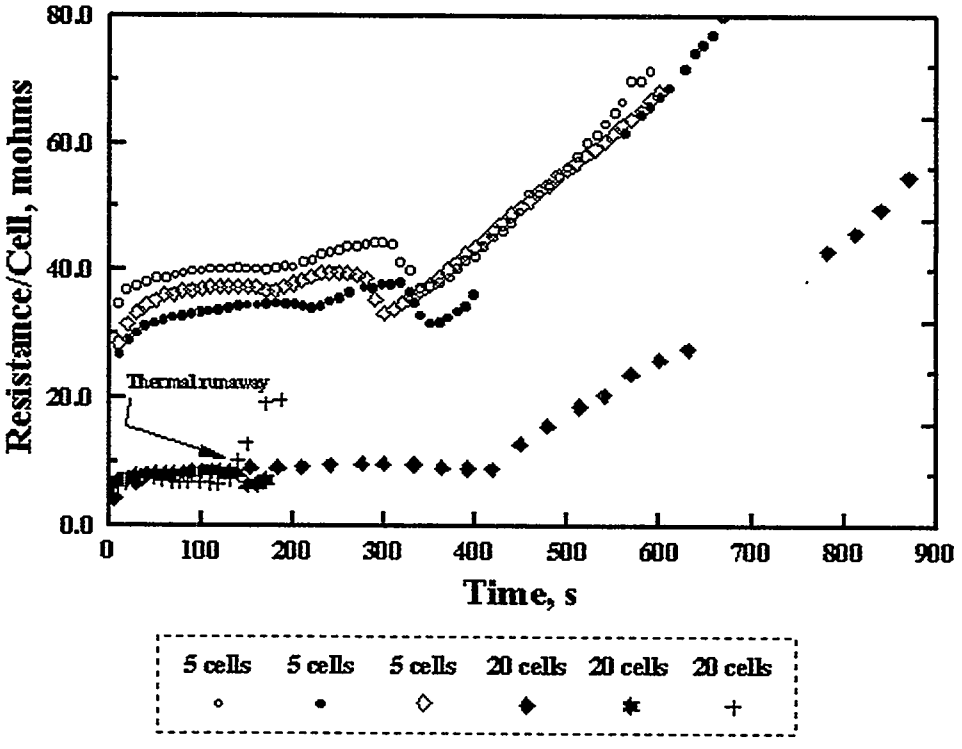


Figure 15. Relative Resistances on a Per-Cell Basis for 1.25"-Dia., 5-Cell and 20-Cell LiSi/LiCl-LiBr-LiF/$CoS_2$ Batteries.

The upper three traces are for the old test fixture that used stainless steel connectors and smaller-gauge wire. The lower traces are for the new text fixture with Cu braid and current collectors. The major difference in the two sets of curves is the reduced IR losses in the new test fixture. This effect is enhanced, as well, by lower interfacial resistance for larger cell stacks.

**20-Cell, 3"-Dia. Batteries.** The next series of tests was carried out using 3"-dia., 5-cell stacks. Two batteries were tested at room temperature with the 4-kW electronic load and a programmed pulse load of ~200 A. This corresponds to a current density of 4.31 A/cm$^2$. The reusable test fixture with the heavy-duty current leads was used and Cu braid was used internally to interface to the external load. The stack was insulated with two 0.08"-thick wraps of ceramic blanket. To minimize IR heating, the batteries were pulsed from open circuit for 1 s every 60 s. The results of the two tests are summarized in Table 3.

Table 3. Summary of Test with 3"-Diameter, 5-Cell Batteries.

| Test No. | Heat Balance, cal/g | Pulse Number | Stack Temp., °C* | No. of Cells | Current Density, A/cm$^2$ | Minimum Voltage/ Cell, V | Power Dens., W/cm$^2$ |
|---|---|---|---|---|---|---|---|
| 1 | 99.4 | 1 | 540 | 5 | 4.31 | 0.714 | 15.4 |
| | | 2 | 535 | | 4.31 | 0.690 | 14.9 |
| | | 3 | 400 | | 4.31 | 0.662 | 14.3 |
| | | 4 | N.A. | | 2.40 | 0.501 | 6.02 |
| 2 | 102.0 | 1 | 550 | 5 | 4.31 | 0.72 | 15.5 |
| | | 2 | 585 | | ---# | --- | --- |
| | | 3 | 600 | | --- | --- | --- |
| | | 4 | 625 | | --- | --- | --- |

* Temperatures taken from temperature-time trace during discharge.
# Load malfunction.

The first battery was able to deliver 196.7 A for the first three pulses, but this dropped to only 109 A (2.4 A/cm$^2$) on the fourth pulse when its voltage dropped below the cutoff value of 6.25V. The battery was also too cold which caused the stack temperature to drop below the freezing point of the electrolyte. The all-Li electrolyte is still a good Li-ion conductor at these temperatures even when it solidifies, which allowed the battery to still deliver a substantial current during the fourth pulse.

The heat balance was increased to 102.0 cal/g for the next 5-cell test with the 3"-dia. stack. After the first pulse, the load malfunctioned so that the data for the remainder of the test was not valid. The temperature profile, however, indicated the higher heat balance was beneficial. The battery resistance was much less than that for the corresponding 1.25"-dia. stacks. The resistance was only 5.8 mΩ/cell for the 3"-dia., 5-cell battery, compared to ~10 mΩ/cell for the 1.25"-dia., 20-cell battery tested in the low-resistance reusable test fixture. This is what is normally observed when small-diameter battery stacks are scaled up in size and number and reflects improved interfacial contact between the cells in the stack.

**125-Cell, 3"-Dia. Batteries.** The next series of tests involved a full-sized module of 125 cells, 3" in diameter. For these tests, a new test fixture was necessary. It used the custom piece parts and feedthroughs shown in Figure 2. The final assembled battery is shown in Figure 16. A close-up view of the header end of the battery is presented in Figure 17. Note the use of the heavy connecting cable and the Cu feedthroughs. The thermocouple is connected to the first cell in the stack adjacent to the base end of the battery opposite the header.

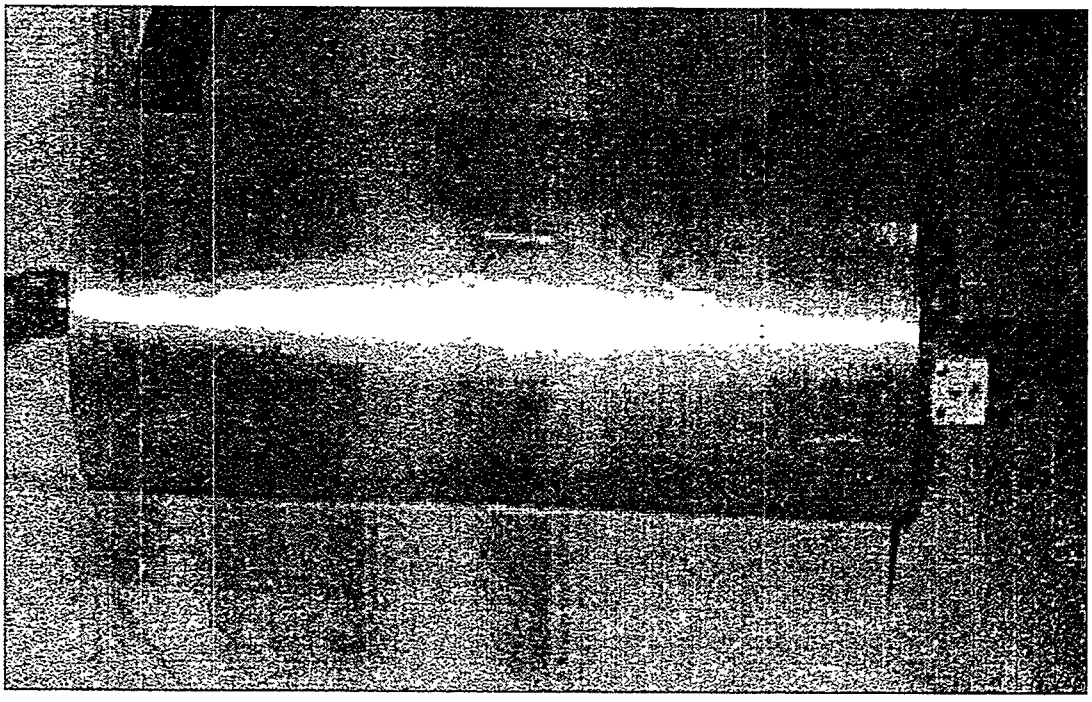

Figure 16. Photograph of Assembled 125-Cell Thermal-Battery Module.

The large power requirements were beyond the capabilities of the existing electronic loads on hand so that an alternate testing method was employed. An Avtron resistive load bank was obtained which was switched across the load with a Kilovac high-power, high-voltage relay. The duration of the applied pulse was controlled through a pulse generator coupled to a high-power switching MOSFET. The experimental setup is shown schematically in Figure 18. A photograph of the experimental setup is shown in Figure 19. For the first test, the load was set at 0.6 ohms which was applied across the load for 1 s every 60 s. This minimized the IR heating in the stack that would have resulted with a continuous load. Heating of the 1/0 Cu cable connected to the battery was not a problem, since it was rated at 400 A continuous.

The battery was activated at room temperature but the load was not applied until 5 s after activation, to allow the stack to heat sufficiently to carry the load. As shown in Figure 20, the rise time to 240 V of ~1.3 s is high but reflects the larger distance for burning of the fuze (heat) strips along the stack during the activation process. The case temperature and the stack

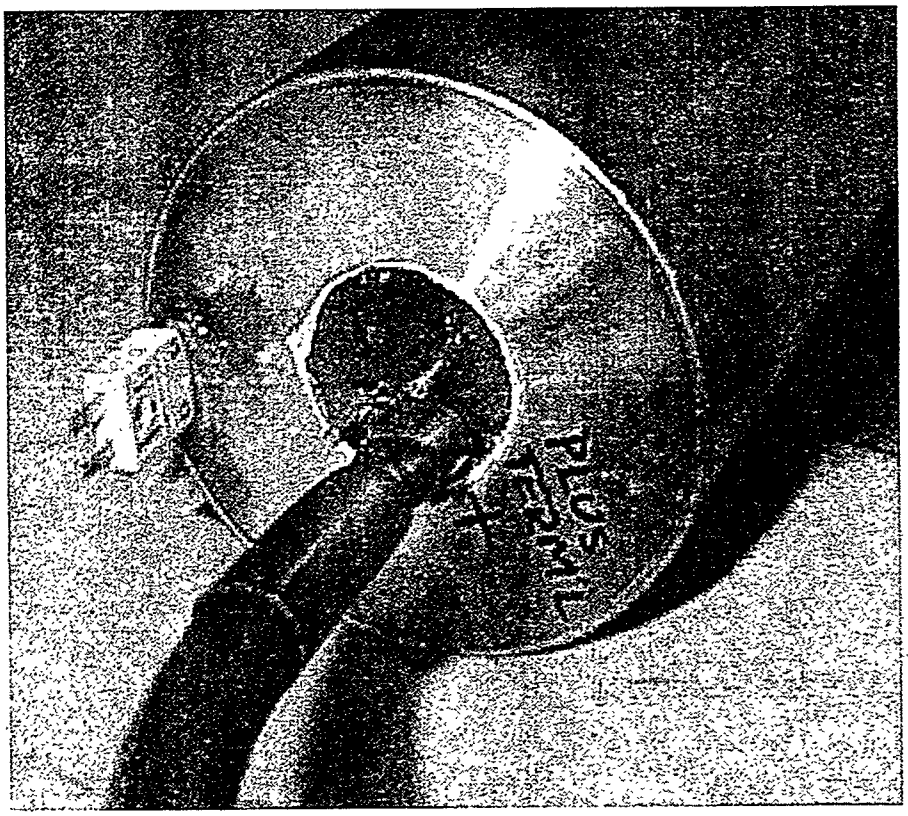

Figure 17. Close-up View of Header End of 125-Cell Thermal-Battery Module.

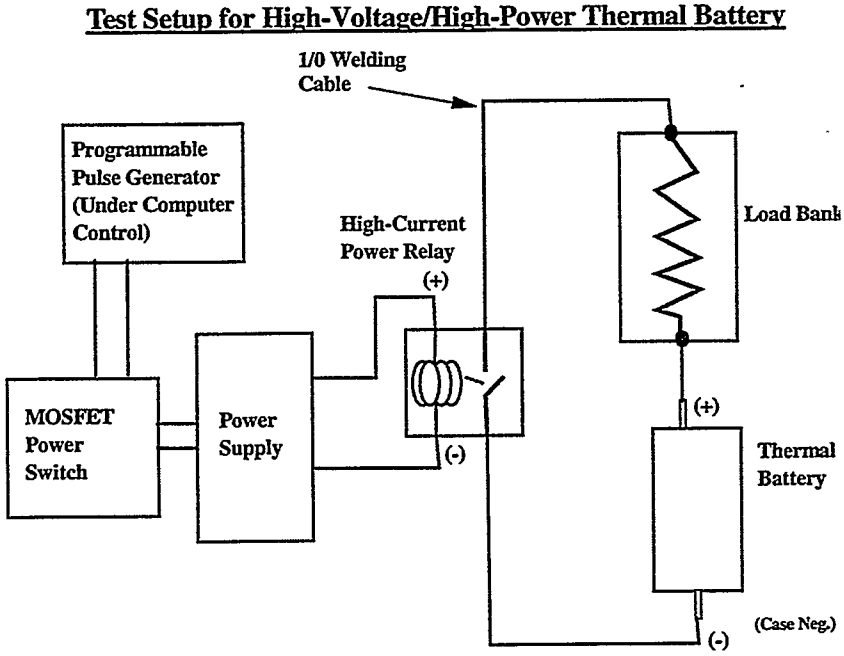


Figure 18. Schematic Representation of Experimental Setup used for testing 125-Cell Thermal-Battery Module.

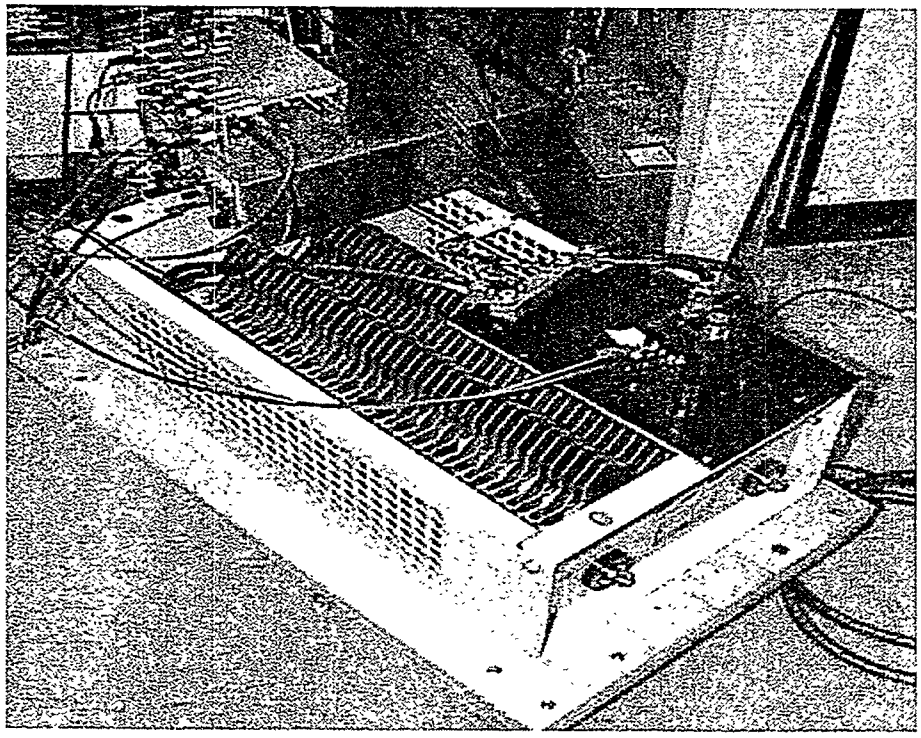

Figure 19. Photograph of Experimental Setup Used to Test 125-Cell Thermal-Battery Module.

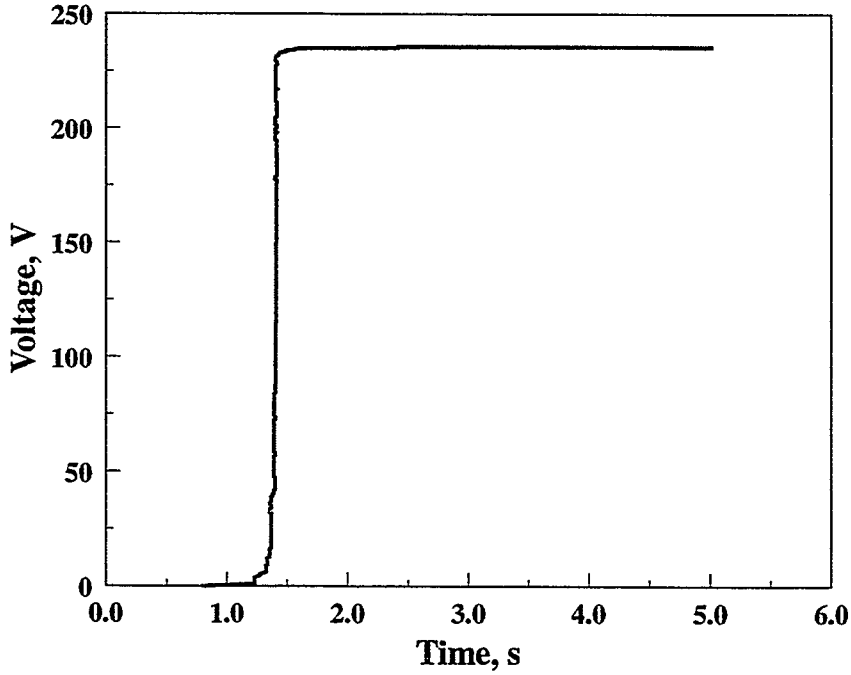


Figure 20. Rise Time while on Open Circuit of 125-Cell Thermal-Battery Module Activated at Room Temperature.

temperature were monitored during the test, to provide an early indicator of the battery experiencing a thermal runaway. As soon as it was obvious that a thermal runaway was starting, liquid nitrogen was to be poured into the test chamber containing the battery, to initiate cooling and control this thermal event.

The steady-state battery voltage during the discharge is shown in Figure 21 for a battery activated at room temperature. There was a rapid drop-off in voltage after ~320 s into the discharge. The resistance of the load bank increased slightly during each pulse, due to IR heating. This was evident in the current and voltage responses during the pulse, especially later in the discharge. The current densities during the second and sixth pulses are shown in Figure 22; the corresponding voltage responses are shown in Figure 23. (For the first two pulses, the duration was limited to 0.5 s for safety concerns. After it was evident that the battery could provide the desired power, the pulse width was increased to 1.0 s.) The drop in the sustainable current density was much greater by the sixth pulse (Figure 22). The voltage drop during the sixth pulse was also greater and there was increased polarization. This is seen by the rounding of the bottom of the voltage trace after the instantaneous voltage drop due to the internal resistance of the battery (Figure 23). The voltage after the sixth pulse also did not return to its pre-pulse level, which is further evidence for increased polarization.

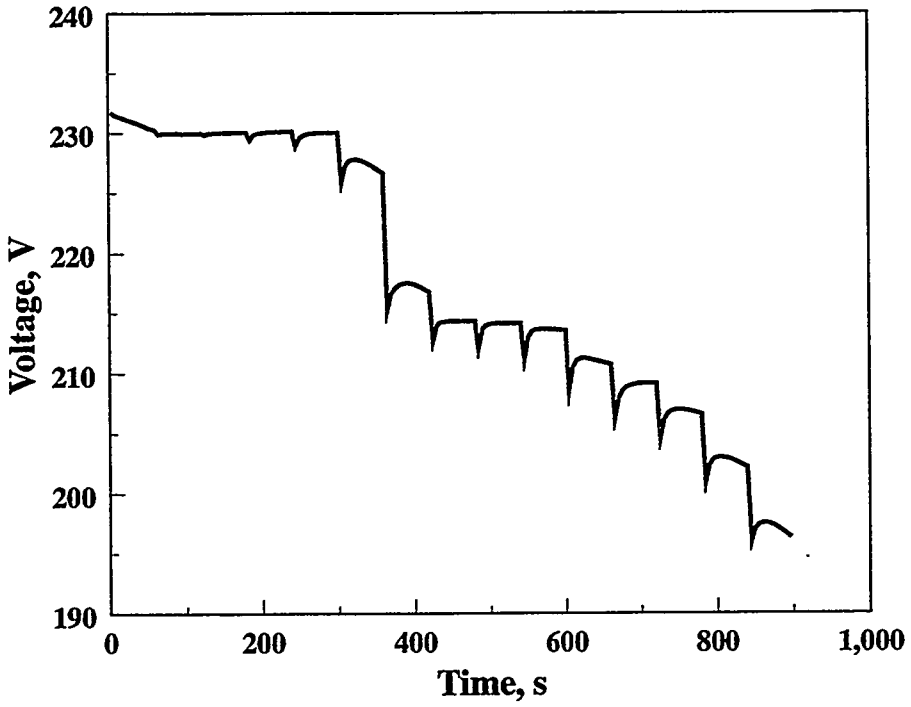


Figure 21. Steady-state Voltage of 125-Cell Thermal Battery Module during Discharge under a 0.6-Ohm Load.

The promising results from this initial test prompted testing of a second 125-cell module but with the resistive load reduced to 0.30 ohms. (The load bank was provided with multiple taps that allowed the resistance to be readily changed.) The battery was pulsed from open circuit every 90 s for 1 s. The time between pulses was increased because of the much higher power

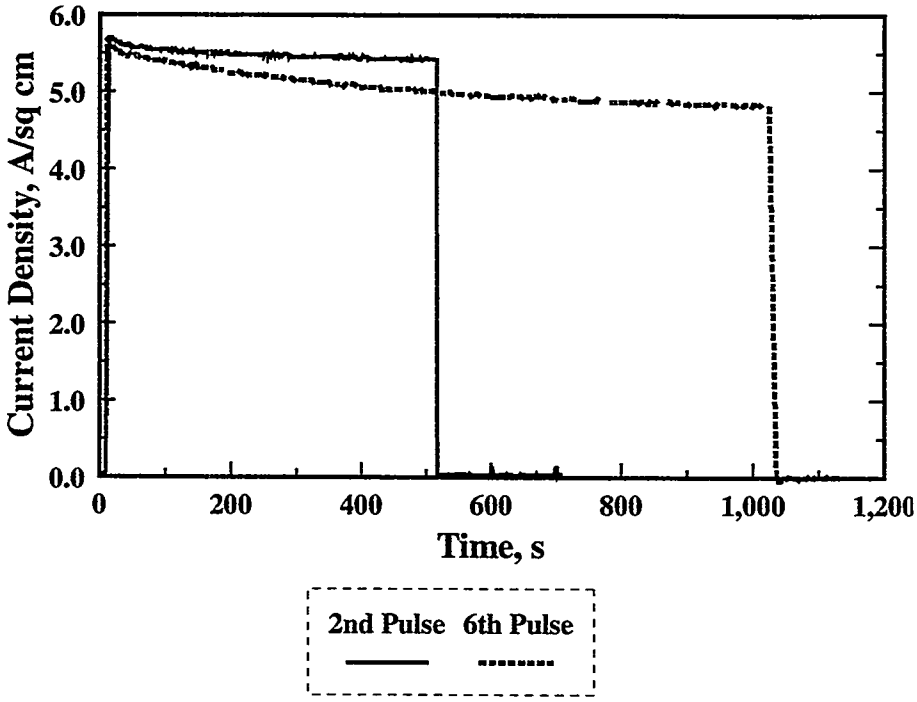


Figure 22. Current Density during Second and Sixth Pulses while Testing of 125-Cell Thermal-Battery Modules under a 0.6-Ohm Load.

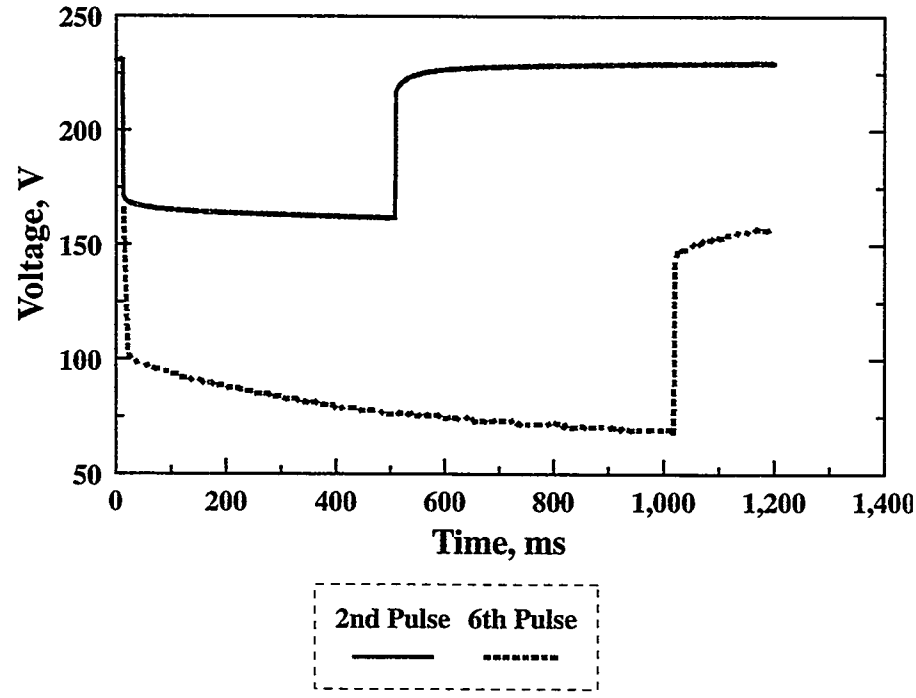


Figure 23. Voltage Response during Second and Sixth Pulses while Testing of 125-Cell Thermal-Battery Modules under a 0.6-Ohm Load.

generated at the lower resistive load. The minimum pulse voltage during discharge is compared for the two batteries in Figure 24. The voltage drop under the 0.30-ohm load was considerably greater than that for the 0.60-ohm load. The initial differences became less with discharge time.

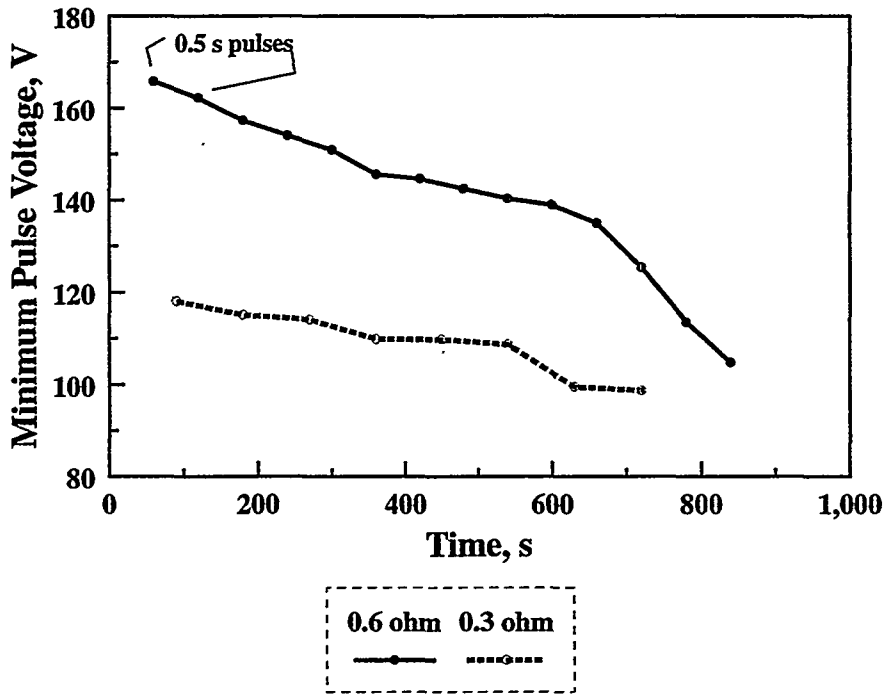


Figure 24. Comparison of Minimum Pulse Voltage for 125-Cell Thermal-Battery Modules Activated at Room Temperature and Tested with 0.60-Ohm and 0.30-Ohm Loads.

As expected, the current drop at the end of the pulse was greater for the case of the 0.30-ohm load. At the first pulse at 90 s, the second battery delivered a current of 350 A, which compares to 262 A for the first battery at 60 s for the 0.60-ohm load. The current densities for the two batteries are compared in Figure 25. Although the load was reduced by half, the current density increased by only 50%. At these low values, the contributions of leads and connections becomes increasingly important. The total polarization of the batteries—including the above resistive contributions—is shown in Figure 26. The overall polarization (resistance) for the battery tested under the 0.30-ohm load was somewhat greater than that for that tested with the 0.60-ohm load.

The real measure of performance for the battery module is the power that is delivered. The power density for the two batteries is compared in Figure 27. The power densities were comparable at the start of discharge for the two batteries. After ~250 s, however, the power density for the battery under 0.30-ohm load was greater until about 600 s, near the end of the run.

The maximum power that was delivered was about 44 kW at the start of discharge, which is less than the desired value of 50 kW. The battery could still deliver over 30-kW pulses after 10 minutes. A level of 40 kW translates into a specific power of 9 kW/kg or 19.2 kW/L for the battery, including all hardware. This is still an impressive achievement.

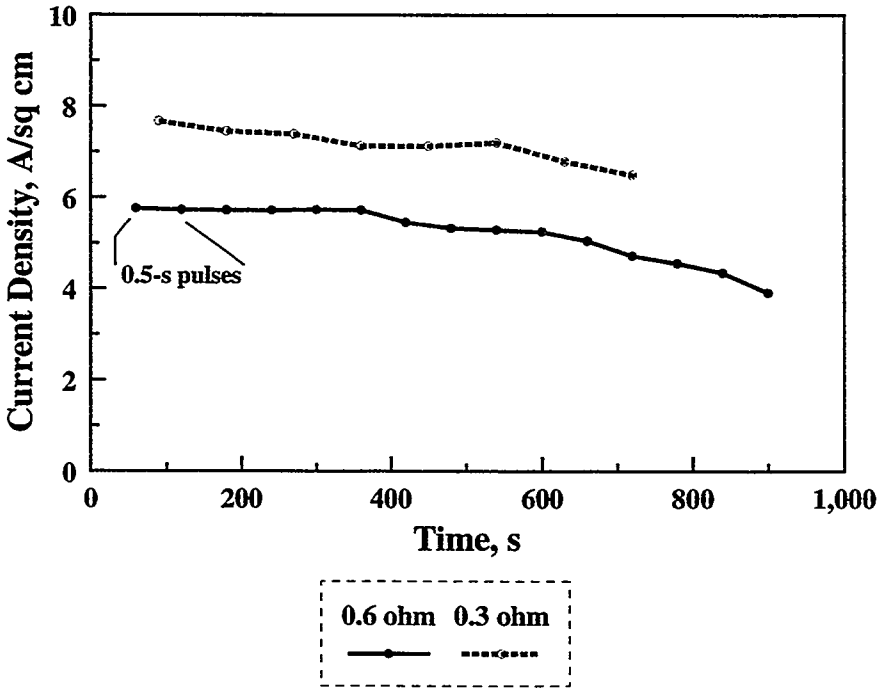


Figure 25. Comparison of Current Density for 125-Cell Thermal-Battery Modules Activated at Room Temperature and Tested with 0.60-Ohm and 0.30-Ohm Loads.

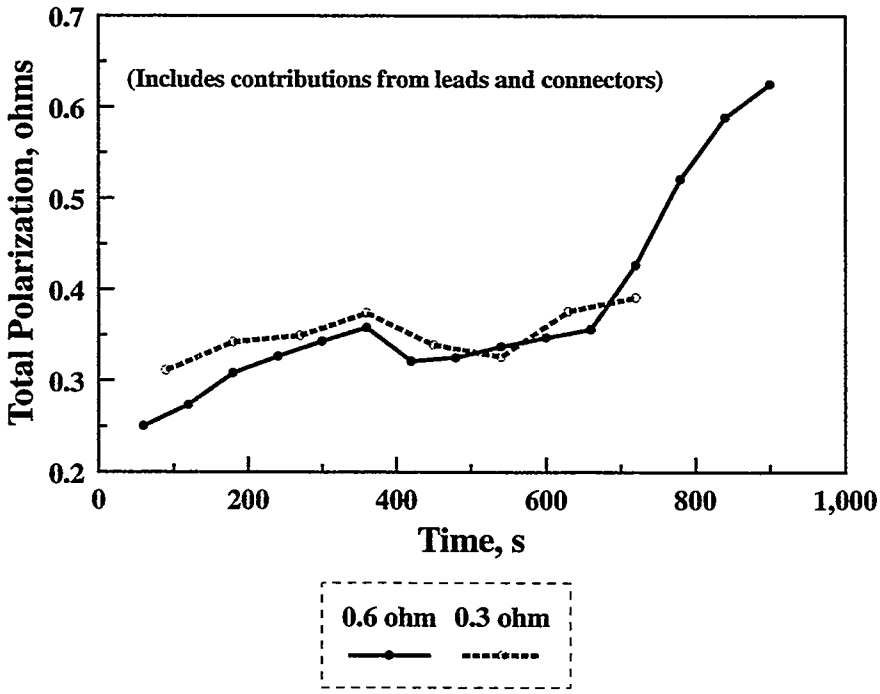


Figure 26. Comparison of Total Polarization for 125-Cell Thermal-Battery Modules Activated at Room Temperature and Tested with 0.60-Ohm and 0.30-Ohm Loads.

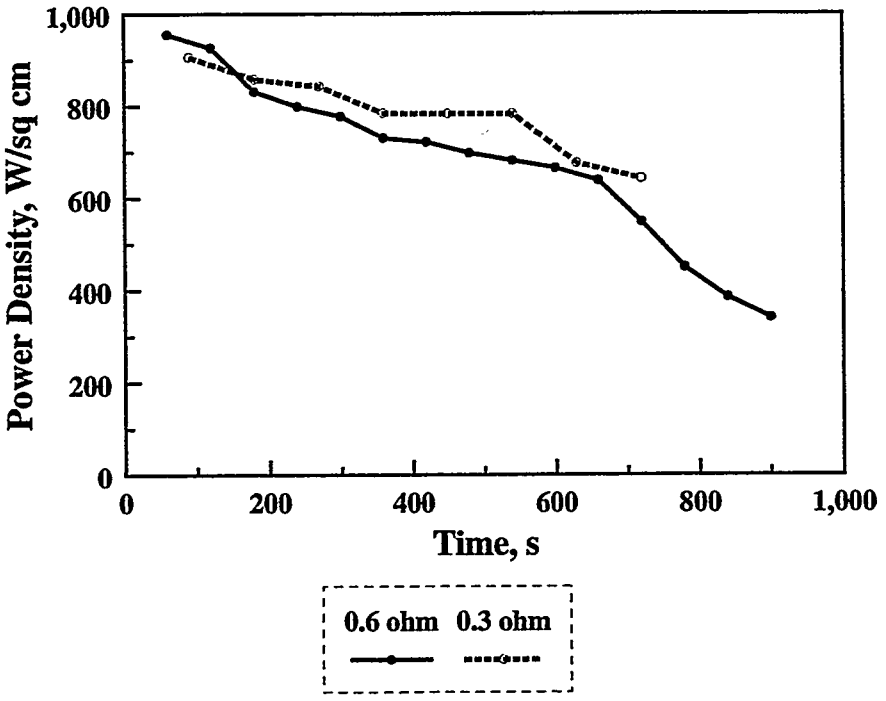


Figure 27. Comparison of Power Density for 125-Cell Thermal-Battery Modules Activated at Room Temperature and Tested with 0.60-Ohm and 0.30-Ohm Loads.

These data indicate that the contributions of the leads and connections are very important for high-power batteries under low resistive loads. A significant percentage of the power dissipation can be associated with this contribution. Designing a battery with minimum internal losses under such high-current discharge conditions becomes increasingly difficult under these conditions. This problem is exacerbated due to the internal self-heating that occurs during the pulsing.

The temperature profiles for the stack and cases for two batteries are compared in Figure 28. There is a substantial increase in stack temperature evident under the 0.30-ohm load because of the higher IR heating relative to the 0.60-ohm load. The case temperature also increased much faster for this battery which ultimately went into a thermal runaway after about 800 s, burning a 1"-dia. hole into the side of the battery case. For the design of this battery module to be considered successful, additional work will be required. The 125-cell modules were tested at ambient conditions. In reality, the battery must be able to function over the entire military temperature range of –54°C to 74°C. The amount of insulation and the heat balance will require further study to ensure that the design is successful from a safety perspective as well as an electrochemical one. The challenges are formidable and will require considerable effort. Because of the lower thermal stability of $FeS_2$, it is highly unlikely that this chemistry can be used with this battery, given the problems encountered with $CoS_2$, which has a decomposition temperature near 650°C, which is 100°C higher than that of $FeS_2$.

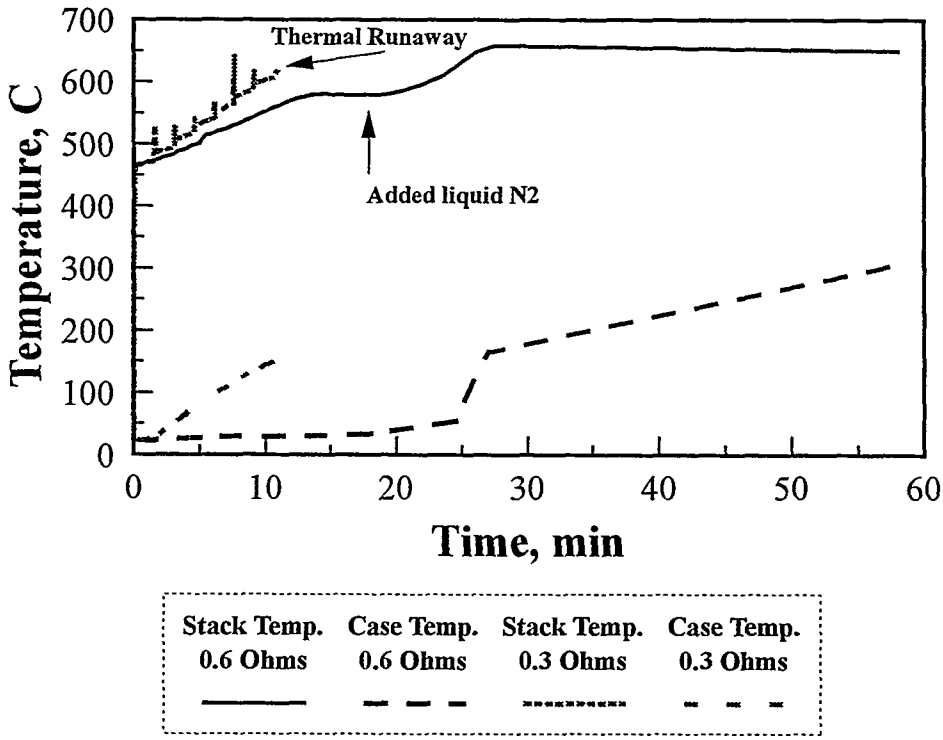


Figure 28. Temperature of Stack and Battery Case for 125-Cell Thermal-Battery Modules Tested with 0.60-Ohm and 0.30-Ohm Loads.

## Conclusions

The capability of a high-power, high-voltage thermal battery was explored by an in-depth electrochemical characterization of the LiSi/LiCl-LiBr-LiF/$CoS_2$ couple. It is not possible to use 1.25"-dia. single cells for characterization purposes due to the failure of the electronic load to regulate at these low voltages. Instead, double and triple cells of this couple, are needed. In a number of isothermal tests, double cells were subjected to increasingly larger current pulses, to determine the maximum current densities that could be obtained. Current densities of 7.7 A/cm$^2$ are realized with triple 0.75"-dia. cells at 550°C. The corresponding power density for these tests is 18.9 W/cm$^2$. However, the coulombic efficiency under these conditions is considerably reduced, relative to lower current densities (e.g., 3.5 A/cm$^2$).

In tests with 1.25"-dia., 5-cell batteries, pulse power densities of 15.0 W/cm$^2$ at 4.8 A/cm$^2$ can be obtained at 104.8 cal/g with Fiberfrax® insulation, under conditions where current limitations are not imposed. A thermal runaway occurs with 20-cell stacks built with Min-K® sleeves at this heat balance when the battery is activated at 74°C. When the heat balance is reduced to 100.2 cal/g, power densities of 250 W/cm$^2$ are delivered at 1-s pulses of 10.1 A/cm$^2$. The battery resistance on a per-cell basis is less for 20-cell stacks than 5-cell stacks. The use of heavy Cu braid and current collectors on the ends of the battery dramatically reduces the internal IR losses.

Limited tests with 3"-dia., 5-cell batteries at 102.0 cal/g show that power densities of 15.5 W/cm$^2$ at 4.3 A/cm$^2$ are readily obtained. The per-cell resistance for 3"-dia. batteries is only 5.8 mohms; this compares to 10 mohms/cell for the 1.25"-dia. batteries.

The final evaluation of 125-cell, 3"-dia. modules shows that the LiSi/LiCl-LiBr-LiF/$CoS_2$ couple can be used to deliver the necessary power for the envisioned application. Pulse current densities of 5.7 A/cm$^2$ (262 A) were obtained when the battery was discharged across a 0.6-ohm load. Early in discharge, the modules are able to deliver over 44 kW of power at power densities of 950 W/cm$^2$ during 1-s pulses. This translates into a specific power of 9 kW/kg or 19.2 kW/L. It is still possible to deliver 30 kW during 1-s pulses after 10 minutes. These data are for batteries activated at room temperature. There is a real danger posed by thermal-runaway of such batteries, as was observed in one instance. Much more work needs to be done with insulation and heat balance before such modules can be safely discharged at their design limits over a temperature range for activation of –54°C to 74°C. Testing such high-voltage and high-power batteries presents a significant challenge in tester design. Internal resistance of leads and contacts can contribute considerably for resistive loads of 0.6 ohms or less.

This study shows that the LiSi/LiCl-LiBr-LiF/$CoS_2$ is a viable candidate for the intended high-voltage, high-power application. The higher thermal stability of $CoS_2$ compared to $FeS_2$ is a key factor in meeting the load requirements while minimizing—though not eliminating—the tendency for thermal runaway.

## References


1. N. Papadakis, G. Barlow, and N. Shuster, *Proc. 37th Power Sources Conf.*, 31 (1996).
2. Ronald A. Guidotti, Gregory L. Scharrer, Edward Binasiewicz, and Frederick W. Reinhardt, *Proc. 38th Power Sources Conf.*, 240 (1998).
3. Ronald A. Guidotti and Frederick W. Reinhardt, "Electrolyte Effects in Li(Si)/$FeS_2$ Thermal Batteries," *Proc. 19th Intern. Power Sources Symp*, 443 (1995).

UNLIMITED DISTRIBUTION

2 Wright Laboratory
Aero Propulsion and Power
Directorate
Att: R. A. Marsh
D. M. Ryan
WL/POOS-2
1950 Fifth St.
Wright-Paterson AFB, OH
45433-7251

1 Argonne National Laboratory
Chemical Technology Div.
Attn: T. Kaun
9700 South Cass Ave.
Argonne, IL 604339

2 Army Research Lab
Attn: F. Krieger
A. Goldberg
2800 Powder Mill Road
Adelphi, MD. 20783

1 A. A. Benderly, Consultant
9915 Logan Dr.
Potomac, Maryland 20854

1 Boeing Aerospace
Attn: Chris Johnson
P. O. Box 3999, M/S 82-32
Seattle, WA 98199

4 Eagle-Picher Technologies, Inc.
Attn: R. Spencer
J. DeGruson
R. Hudson
C. Lamb
P.O. Box 47
Joplin, MO 64802

1 Technochem Co.
Attn: Shyam Argade
203A Creekridge Rd.
Greensboro, NC 27406

4 Enser Corp.
Attn: J. Ronacher
N. Shuster
N. Miller
J. Cubero
P.O. Box Drawer 48548
St. Petersburg, FL 33743-8548

1 Naval Ordnance Station
Attn: K. Englander
Code 5123C
Indian Head, MD 20640

2 Naval Surface Warfare Center
Attn: B. Larrick
C. E. Mueller
Silver Springs, MD. 20910

1 Naval Surface Warfare Center
Attn: C. Winchester
Code 683, Electrochemistry
Branch
9500 McArthur Blvd.
W. Bethesda, MD 20817-5700

3 Naval Weapons Center
Attn: M. H. Miles
R. Nolan (Code 3626)
D. Rosenlof (Code 3626)
China Lake, Ca 93555

1 Parker Hannifin
Attn: Arvind Ahluwalia, MS K141
14300 Alton Parkway
Irvine, CA 92718-1814

1 SAFT America
Attn: K. K. Press
Doug Briscoe
107 Beaver Court
Cockeysville, MD 21030

1 Jim O'Loughlin
USAF Phillips Laboratory, HERTF,
PL/WSTI
6550 Aberdeen Ave.
KAFB Building 66071, Rm 125
Alb, NM 87117-5776

2 DRA Haslar
Materials Dept.
Attn: J. Knight
A. G. Ritchie
Gosport
Room F8, AC Building
Hampshire PO 12 2AG
ENGLAND

1 Leclanche, S.A.
Attn: P. Reutschi
48, Avenue de Grandson
CH-1401 Yverdon-Les-Bain
SWITZERLAND

1 ASB
Att: A. J. Clark
Allée Ste Hélène
18000 BOURGES CEDEX
FRANCE

1 MS0614 P. C. Butler, 2522
1 MS0614 A. H. Andazola, 2522
1 MS0614 F. P. Lasky, 2522
1 MS0614 F. W. Reinhardt,2522
5 MS0614 R. A. Guidotti, 2522
1 MS0614 R. W. Bickes, 2523
1 MS0614 L. M. Moya, 2523
1 MS0614 L. Demo, 2523
1 MS0614 J. A. Gilbert, 2523
1 MS1453 G. L. Scharrer, 2553
1 MS9018 Central Technical Files, 8490-2
2 MS0899 Technical Library, 4616
1 MS0612 Review Approval Desk, 4912
for DOE/OSTI